Concentration dependence of absorption and optical and hyperfine transition dynamics in Pr^{3+}:$La_2(WO_4)_3$

2012 J. Phys. B: At. Mol. Opt. Phys. 45 124014

(http://iopscience.iop.org/0953-4075/45/12/124014)

J. Phys. B: At. Mol. Opt. Phys. **45** (2012) 124014 (7pp) doi:10.1088/0953-4075/45/12/124014

Concentration dependence of absorption and optical and hyperfine transition dynamics in Pr^{3+}:$La_2(WO_4)_3$

F Beaudoux, O Guillot-Noël[1], J Lejay, A Ferrier and P Goldner

Laboratoire de Chimie de la Matière Condensée de Paris, Chimie-Paristech, CNRS UMR 7574, UPMC Univ Paris 06, 11, rue Pierre et Marie Curie, F-75005 Paris, France

E-mail: philippe-goldner@chimie-paristech.fr

Received 20 December 2011, in final form 27 February 2012
Published 8 June 2011
Online at stacks.iop.org/JPhysB/45/124014

Abstract

Optical and hyperfine parameters of the $^3H_4$–$^1D_2$ transition are investigated in Pr^{3+}:$La_2(WO_4)_3$ for doping concentrations ranging from 0.02 to 3 at.%, at liquid helium temperatures. This includes optical inhomogeneous and homogeneous linewidths, peak absorption, excited-state population decays, spectral hole lifetime and inhomogeneous and homogeneous hyperfine linewidths. Optical inhomogeneous broadening with increasing Pr^{3+} concentration is limited due to close atomic radii between Pr^{3+} and La^{3+}. The peak absorption coefficient increases with increasing Pr^{3+} doping, reaching up to 28 cm^{-1}. At the highest Pr^{3+} concentration, optical coherence lifetime is 4.6 μs and hole lifetime 2 s, which should allow one to transfer coherences and tailor the optical inhomogeneous linewidth, as required for rare earth-based optical quantum memories. Raman echo experiments show that hyperfine inhomogeneous linewidth and coherence lifetime (50 kHz and 250 μs respectively) are independent of Pr^{3+} concentration. These results suggest that highly doped crystals are useful for efficient and long-storage time quantum memories.

1. Introduction

Rare earth ions embedded in single crystals can exhibit optical transitions with long coherence lifetimes at liquid helium temperatures [1]. This is explained by the shielding of 4f electrons by closed $5s^2$ and $5p^6$ shells which result in atomic-like properties for these solid-state systems. As an example, a homogeneous linewidth of 73 Hz has been measured in Er^{3+}:Y_2SiO_5, corresponding to a coherence lifetime of 4.4 ms [2]. Moreover, several rare earth ions (e.g. Pr^{3+}, Nd^{3+}, Eu^{3+}, Er^{3+} and Tm^{3+}) have isotopes with nonzero nuclear spins, which allows one to take advantage of hyperfine transitions with even longer coherence lifetimes. Using specific magnetic fields [3, 4] and radio-frequency decoupling pulses [5], it is possible to extend hyperfine coherence lifetimes by two to four orders of magnitude up to a few 10 s. These properties suggest that rare earth-doped crystals are well suited for designing optical quantum memories with long storage times. Indeed, many promising experimental and theoretical results have been reported in this field. In particular, efficient, multi-mode protocols, derived from schemes of photon echoes (i.e. using optical coherences), have been proposed [6–9] and tested, sometimes with quantum fields, in Pr^{3+}:Y_2SiO_5 [10, 11], Tm^{3+}:$Y_3Al_5O_{12}$ [9, 12], Tm^{3+}:$LiNbO_3$ [13], Er^{3+}:Y_2SiO_5 [9, 14], Nd^{3+}:YVO_4 [8] and Nd^{3+}:Y_2SiO_5 [15, 16]. Despite these promising demonstrations, it has not yet been possible to demonstrate an efficient, long-storage, high-bandwidth quantum memory in a unique material. High efficiency is one important issue since it requires very large optical density for the absorbing transition. As rare earth f–f transitions are essentially forbidden, oscillator strengths are low (10^{-8}–10^{-6}), and large optical densities are difficult to obtain. This could be solved in several ways, like using tuned cavities [17], waveguides or highly doped samples. Increasing absorption by increasing doping is however only possible if the dopant does not create too many strains in the host so that the inhomogeneous linewidth remains small. Otherwise, peak absorption stays more or less constant with increasing dopant

[1] In memoriam.

concentration, as shown in Eu^{3+}:Y_2SiO_5 [18]. This broadening can be related to ionic radius difference between the dopant and the host cation which is substituted. In Y_2SiO_5, Pr^{3+} substitutes Y^{3+}, which has a smaller ionic radius ($r_{Pr^{3+}} = 1.14$ Å and $r_{Y^{3+}} = 1.02$ Å [19]), resulting in high doping-related strains and fast increase of inhomogeneous linewidth with Pr^{3+} concentration. In order to overcome this limitation, we developed a lanthanum-based crystal, Pr^{3+}:$La_2(WO_4)_3$, since La^{3+} and Pr^{3+} have closer atomic radii : $r_{La^{3+}} = 1.18$ Å. Pr^{3+} optical and hyperfine transitions were studied and parameters such as optical inhomogeneous linewidth and dephasing time were determined [20]. Hyperfine transitions were also studied, showing that despite the high magnetic moment of lanthanum, hyperfine coherence lifetimes were long, around 250 μs [21]. Moreover, efficient electromagnetically induced transparency, another quantum memory protocol, was observed in this material, with narrow transparency windows and light velocity down to 17 km s^{-1}, in very good agreement with theory [22]. Recently, we also characterized ground- and excited-state spin Hamiltonians and used zero first-order Zeeman shift transitions [3] to demonstrate a 630-fold increase in hyperfine coherence lifetimes, the latter reaching 158 ms for an optimized magnetic field [4]. Crystal field calculations were performed, showing that principal values of hyperfine interaction tensors can be well predicted [4, 23].

In this paper, we first investigate absorption dependence on Pr^{3+}concentration in $La_2(WO_4)_3$ and find that peak absorption is indeed increasing with increasing doping, with limited inhomogeneous broadening. We then consider other parameters important for quantum memories: optical population and coherence lifetimes, spectral hole lifetimes and hyperfine coherence lifetimes as well as inhomogeneous linewidths. The results show that 3% at. Pr^{3+}-doped samples still exhibit good properties, with hyperfine coherence lifetimes similar to low concentration crystals and spectral hole and optical coherence lifetimes compatible with spectral tailoring and coherence transfer.

2. Experimental details

$La_2(WO_4)_3$ is a monoclinic crystal where La^{3+} ions occupy one site of C_1 symmetry. Samples with Pr^{3+} atomic concentrations of 0.02% , 0.2% , 1.4% and 3% (corresponding, respectively, to 1.6×10^{18}, 1.6×10^{19}, 1.09×10^{20} and 2×10^{20} ions cm^{-3}) were grown by the Czochralski method. Experiments were performed on the $^3H_4 \rightarrow {}^1D_2$ transition between the lowest energy crystal field levels of each multiplet, at 602.74 nm (vacuum). Light propagated along the $b(C_2)$ crystal axis with polarization adjusted in the a, c plane for maximum absorption. Crystals with thickness of 1–5 mm were placed into a helium bath Janis cryostat at 3.5 K. Excitation was provided by a Coherent 899–21 frequency-stabilized dye laser (1 MHz linewidth) gated by an AA optoelectronics 110 MHz acousto optic modulator (AOM) in a double-pass configuration. Absorption was measured using a low-power (150 μW) large-diameter (2 mm) beam to avoid saturation effects. A signal was detected by a Thorlabs PDB 150A amplified silicon photodiode. Hole lifetimes were measured by burning at a fixed frequency for 1 ms and, after a variable delay, scanning 100 MHz in 100–600 μs in a single shot around this frequency. Laser intensity was reduced by 1000 during the scan to avoid ground-state population redistribution. Photon echoes were recorded by focusing the laser to a 150 μm spot with powers up to a few 10 mW. Pulses were 1 μs long. To avoid hole burning, the laser was slowly scanned (in $\approx$ 1 s) over 1 GHz. Echoes were detected by a Hamamatsu C5460 avalanche photodiode gated by an AOM to prevent detector damage or saturation. For Raman echo experiments, two-colour pulses were created by using separate optical paths, each containing an AOM in a double-pass configuration. The frequency-shifted beams were then combined on a beam splitter and injected in a single-mode, polarization-maintaining, fibre, in order to ensure mode cleaning and high overlap. The laser powers at the sample were $\approx$ 8 mW and the pulses 3 μs long. Raman echoes were detected using a heterodyne scheme (see section 4.2) with a 10 μs pulse and the silicon photodiode set to a bandwidth of 50 MHz. Fluorescence decays were measured using an OPO pumped by a tripled YAG (BMI) which produced 8 ns pulses. The signal was analysed by a 25 cm focal length Jobin Yvon monochromator and an intensified CCD camera (Princeton Instruments). For these experiments, samples were mounted into a helium closed-cycle cryostat and cooled down to 10 K.

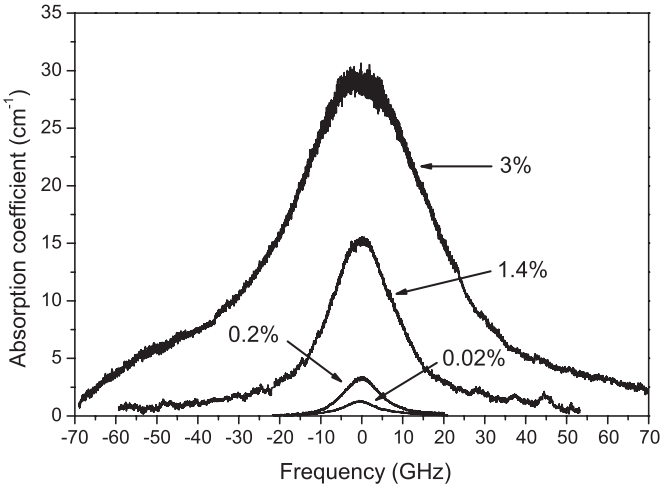

Figure 1. Absorption spectra of the $^3H_4 \rightarrow {}^1D_2$ transition as a function of Pr^{3+} concentration. T = 3.5 K.

3. Absorption

Figure 1 presents absorption spectra of the $^3H_4 \rightarrow {}^1D_2$ transition as a function of Pr^{3+} concentration. Peak absorptions and full widths at half-maximum are reported in figure 2. The inhomogeneous linewidth increases linearly with Pr^{3+} concentration with a slope of 10.8 GHz/at.% or 1.6 GHz/(10^{19} cm^{-3}). This is about 12 times less than what is observed in Pr^{3+}:Y_2SiO_5 [24, 25], showing that ionic radius difference has indeed a large influence. The low strain induced by Pr^{3+} doping was also confirmed by determining crystal cell parameters by x-ray diffraction and Rietveld refinement. A linear dependence of parameters on Pr^{3+} concentration was

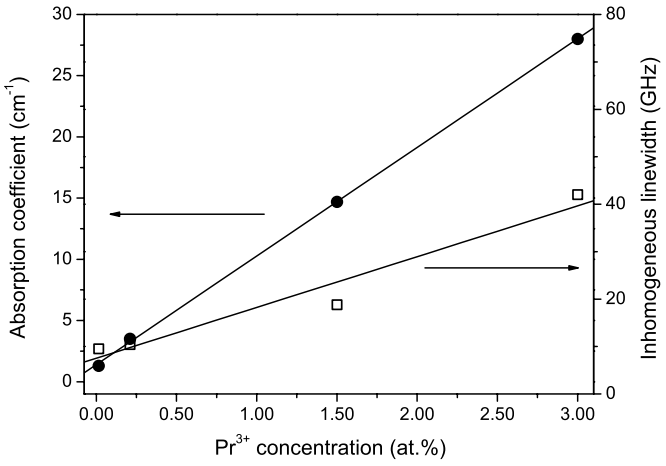

Figure 2. Peak absorption coefficient (circles) and inhomogeneous broadening (open squares, full width at half-maximum) of the $^3H_4 \rightarrow {}^1D_2$ transition as a function of Pr^{3+} concentration.

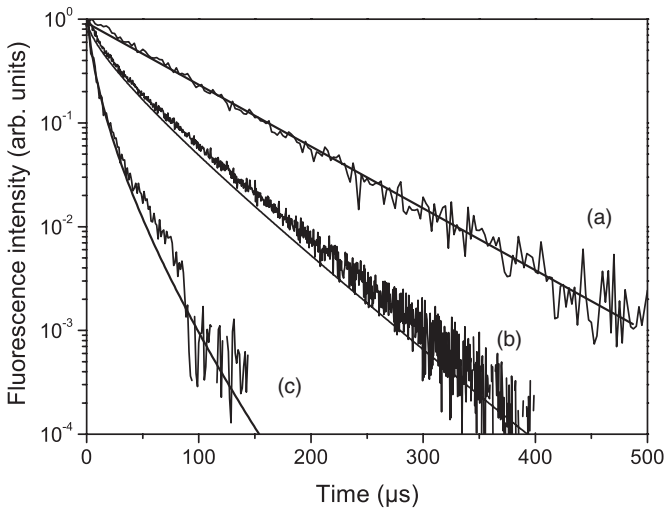

Figure 3. $^1D_2 \rightarrow {}^3H_4$ fluorescence decay as a function of Pr^{3+} concentration (a) 0.02 at.%, (b) 1.4 at.% and (c) 3 at.%. T = 10 K.

found, corresponding to a small contraction of the cell (Pr^{3+} ions being smaller than La^{3+} ions) of 0.33 Å^3/at.%. At the lowest Pr^{3+} concentration, 0.02 at.%, the inhomogeneous linewidth is however still quite large (Γ_{inh} = 9 GHz) in comparison with 0.02 at.% Pr^{3+}:Y_2SiO_5 (Γ_{inh} = 4.4 GHz [25]). This could be due to the growth parameters, which were not fully optimized. Tungstate oxide evaporation during the growth which continuously modifies liquid composition could also induce defects in the crystal.

The peak absorption coefficient has also a linear dependence on Pr^{3+} concentration, reaching 28 cm^{-1} in the 3 at.%-doped sample. We noted a variation of the oscillator strength f_c of the transition with concentration, suggesting a link between site distortion and transition strength, which is however difficult to analyse given the low undistorted La^{3+} site symmetry (C_1). Oscillator strengths are weak, with values in the 2–4 $\times 10^{-8}$ range, about one order of magnitude smaller than in Pr^{3+}:Y_2SiO_5. Finally, the lines could be well fitted with a Lorentzian function at all concentrations, which is consistent with Pr^{3+} point defects [18].

4. Population and coherence lifetimes

In this section, the dynamics of optical and hyperfine transitions are studied with respect to population and coherence lifetimes. If the latter importance for quantum memories is obvious since they, respectively, allow the optical to spin coherence transfer and determine the storage time of the memory, population lifetimes are also crucial parameters [26, 27]. This is because quantum memory protocols require tailoring of the inhomogeneous lineshape which can be efficiently done through optical pumping only if the ground-state hyperfine population lifetimes are much longer than the optical excited-state one.

4.1. Optical transition

Homogeneous linewidths (Γ_h) of optical transitions in rare earth-doped single crystals at low temperature (<4 K) are determined by contributions from the excited-state population lifetimes (Γ_{pop}), instantaneous spectral diffusion (ISD) (Γ_{ISD}) and the host spins, including Pr^{3+} nuclear spin, ($\Gamma_{ion-host}$) [28]. In the following, these contributions are separately studied. The coherence lifetime T_2 is related to the homogeneous linewidth by $T_2 = 1/(\pi\Gamma_h)$.

Fluorescence decays of the $^1D_2 \rightarrow {}^3H_4$ transition are shown in figure 3. Exponential behaviour is observed for the 0.02- and 0.2 at.%-doped samples with a corresponding lifetime for the $^1D_2$ level of 64 μs, which can be assumed to be of radiative nature because of the large energy gap (6500 cm^{-1}) between the $^1D_2$ and $^1G_4$ levels. At higher concentrations, a clear non-exponential behaviour appears which is attributed to Pr^{3+}–Pr^{3+} energy transfer ($^1D_2$,$^3H_4$)$\rightarrow$($^1G_4$,$^3F_4$) [20]. Because of the inhomogeneous to homogeneous linewidths ratio ($\geqslant 5 \times 10^5$), resonant energy migration among Pr^{3+} ions can be neglected. The decays can therefore be analysed by the Inokuti–Hirayama model [29]. The fluorescence intensity $I(t)$ is given by

$$I(t) = I_0 \exp\left[-\frac{t}{\tau_0} - \Gamma\left(1-\frac{3}{s}\right)\frac{N}{C_0}\left(\frac{t}{\tau_0}\right)^{3/s}\right], \qquad (1)$$

where τ_0 is the excited-state lifetime without energy transfer, that was determined at low Pr^{3+} concentrations, Γ is the gamma function, s is a parameter depending on the multipolar degree of the interaction, N is the Pr^{3+} concentration and C_0 is the critical concentration. The critical concentration is related to the critical distance R_0 by $C_0 = 3/(4\pi R_0^3)$, the latter being defined as the distance for which the transfer rate is equal to the spontaneous decay one. The model fits reasonably well the experimental curves for $s = 6$, in agreement with electric dipole–dipole interactions and giving R_0 = 1 nm for the 1.4- and 3 at.%-doped samples. In the latter case, the critical and average distances between ions ($R_{av} = (4\pi N/3)^{-1/3}$ nm) are equal, in qualitative agreement with the fast decay observed for this sample.

Homogeneous linewidths were determined from two-photon echo decay curves, which were found to follow an exponential law. Reliable values for the homogeneous

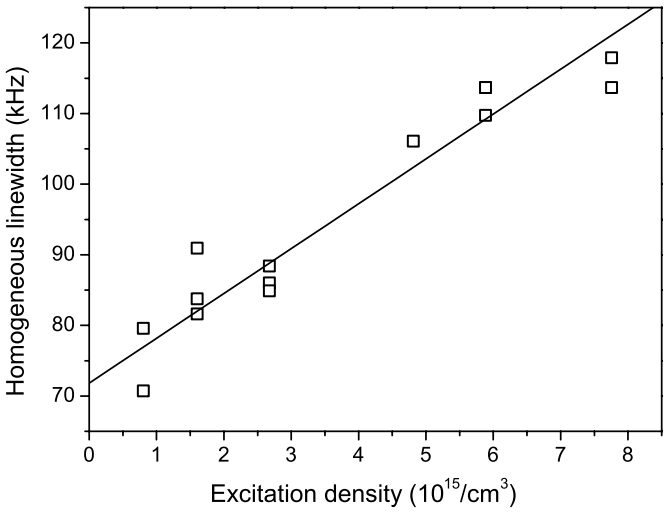

Figure 4. Homogeneous linewidth of the $^3H_4$–$^1D_2$ transition as a function of the excitation density in 3 at.% Pr^{3+}:$La_2(WO_4)_3$ at 3.5 K.

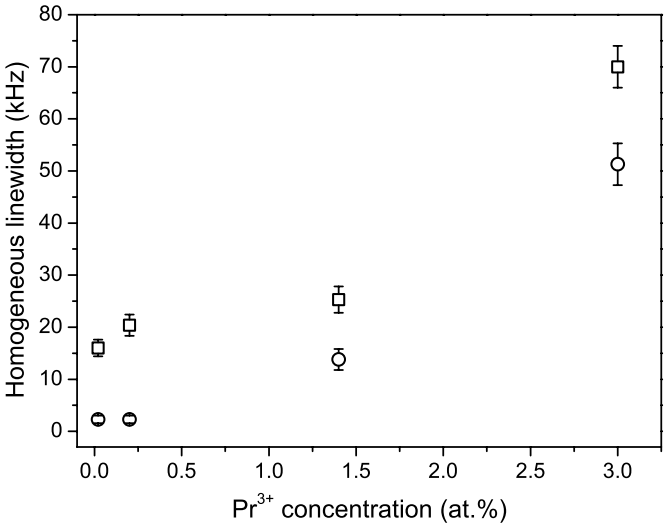

Figure 5. Homogeneous linewidth (Γ_h, open squares) of the $^3H_4$–$^1D_2$ transition and contribution from the excited-state population lifetime (Γ_{pop}, open circles) as a function of Pr^{3+} concentration.

linewidths were obtained with the following procedure: the linewidths were determined for different excitation densities and extrapolated linearly to zero excitation density (figure 4). This procedure was necessary because of ISD caused by the rephasing pulse. The latter drives ions to the excited state, which has generally a different permanent electric dipole moment than the ground state. This is especially true for low site symmetries. This change in dipole moment shifts the frequency of neighbouring ions which therefore cannot rephase and cannot contribute to the echo intensity. This effect increases with increasing number of excited ions and therefore with laser intensity and ion concentration. The ISD contribution to the homogeneous linewidth, Γ_{ISD}, is proportional to the excitation density ρ_e

$$\Gamma_{ISD} = S_{ISD}\rho_e, \tag{2}$$

where ρ_e is related to the excitation intensity I, the excited-state lifetime T_1 and the absorption coefficient α by $\rho_e = 3 \times 10^{12} I T_1 \alpha$ [18]. Since the echo signal went essentially to zero after 20 μs, the decay curves were fitted by simple exponentials on this time range to determine the T_1 values. I is given by $I = 2P/\pi\omega_0^2$, where P is the laser power and ω_0 is the beam waist. The S_{ISD} parameter varies from 3 to 6×10^{-12} Hz cm^{-3} when Pr^{3+} concentration increases from 0.02 to 3 at.%. These values are lower than those measured in Pr^{3+}:Y_2SiO_5 and Pr^{3+}:$KY(WO_4)_2$ (1.2×10^{-11} and 3.5×10^{-11} Hz cm^{-3}, respectively).

The concentration dependence of the homogeneous linewidth extrapolated at zero excitation intensity is presented in figure 5 together with the contribution Γ_{pop} of the excited-state lifetime. The latter was calculated from the initial decay of the fluorescence, as in the case of the ISD experiments (see above), using $\Gamma_{pop} = 1/(2\pi T_1)$. The homogeneous linewidth ranges from 16 kHz ($T_2 = 20$ μs) to 70 kHz ($T_2 = 4.5$ μs) as Pr^{3+} concentration is increased. This variation is mainly due to the excited-state lifetime contribution which is negligible at low Pr^{3+} concentration ($\Gamma_{pop} \approx 2.5$ kHz) but reaches 73% of Γ_h in the 3%-doped sample ($\Gamma_{pop} \approx 52$ kHz). Figure 5 also shows that the contribution not related to the excited-state lifetime, $\Gamma_{ion-host} = \Gamma_h - \Gamma_{pop}$, is nearly independent of Pr^{3+} concentration, at least in the range studied here. This indicates that Pr^{3+} dephasing is due to interactions with the host, probably $^{139}La^{3+}$ nuclear spins (I = 7/2, 99.91% abundance, 2.78 μ_B magnetic moment). This is confirmed by the study of hyperfine transition coherence lifetimes (see section 4.2).

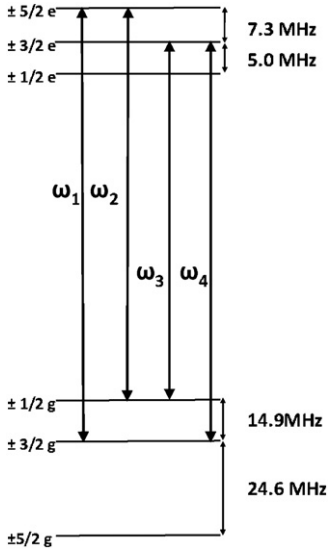

Figure 6. $^3H_4$ and $^1D_2$ level hyperfine structure in Pr^{3+}:$La_2(WO_4)_3$ and transitions used in the Raman echo experiments.

4.2. Hyperfine transition

Praseodymium has a 100% abundant isotope, $^{141}Pr^{3+}$, with a 5/2 nuclear spin. The zero-field hyperfine splittings have been determined by hole burning spectroscopy [20] and level ordering by spectral tailoring [21]. The ground- and excited-state hyperfine structures are shown in figure 6.

We first determined the average lifetime of the ground-state hyperfine levels by burning a spectral hole in the

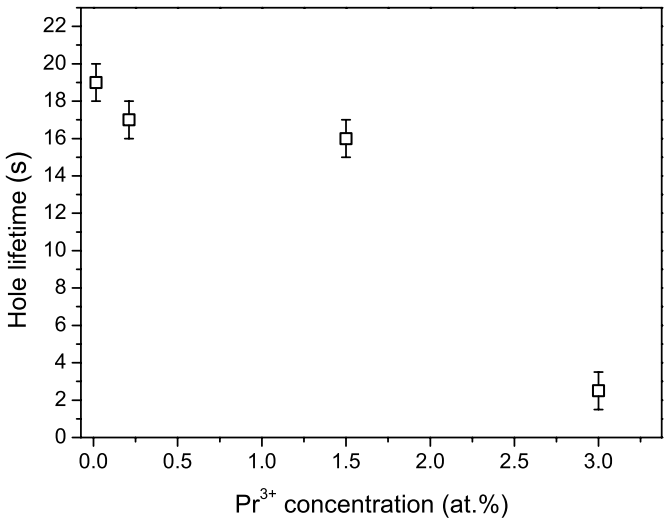

Figure 7. Hole lifetime as a function of Pr^{3+} concentration.

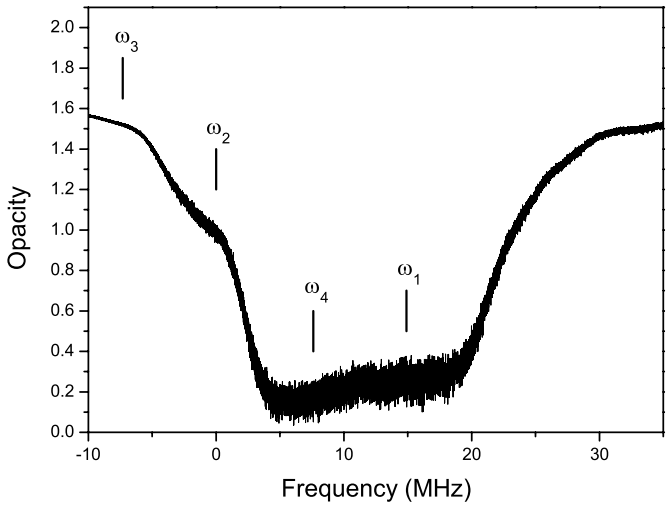

Figure 8. Transition frequencies and spectral hole used for the Raman echo experiments.

inhomogeneous linewidth and observing its decay, which was found to be exponential. Holes have a much longer lifetime than the optical excited state and are due to a population redistribution among the hyperfine ground-state levels. Their decay time corresponds therefore to an average relaxation time T_1^{hyp} between hyperfine levels. Figure 7 presents the hole lifetime as a function of Pr^{3+} concentration. Until 1.4 at.%, the value is in the 16–19 s range but drops to 2 s at 3%. This suggests an onset of a flip-flop process when the average Pr^{3+}–Pr^{3+} distance is around 1 nm. We note however that the rate of this process is still very slow and is unlikely to affect hyperfine coherence lifetimes (see below). As stated above, efficient optical pumping requires high ratios between ground-state hyperfine and optical excited-state population lifetimes (T_1^{hyp} and T_1, respectively). More precisely, the ratio r between populated and depopulated levels in the ground state reads [26]

$$r = 1 + \frac{2T_1^{\mathrm{hyp}}}{T_1}. \tag{3}$$

Even for the 3% Pr^{3+}-doped sample, $r \approx 4 \times 10^5$ (taking $T_1 = 10\ \mu$s at long times) which allows one to easily burn holes with 100% transmission, as it was experimentally observed.

Coherence lifetimes were studied using the Raman echo technique which consists in optically exciting, rephasing and detecting spin echoes [30–32]. We investigated the $\pm 1/2$–$\pm 3/2$ ground-state transition which lies at 14.870(1) MHz at zero magnetic field [4]. The two-colour beam used to excite and rephase the spin coherence was set along the strong $\pm 3/2$g–$\pm 5/2$e and $\pm 1/2$g–$\pm 5/2$e transitions (g and e labels indicate ground and excited states, respectively) [21]. The corresponding frequencies are ω_1 and ω_2 (figure 6). To create a large spin coherence, it is necessary to have a large population difference between the corresponding levels. For this purpose, a large hole ($\approx$ 16 MHz) was burned into the inhomogeneous linewidth in order to empty, for some classes of ions, the $\pm 3/2$g level (figure 8). Detection was performed by sending a probe pulse along the $\pm 1/2$g–$\pm 3/2$e transition (at ω_3 frequency) which induced an optical coherence along the $\pm 3/2$g–$\pm 3/2$e transition at frequency ω_4 because of the spin coherence

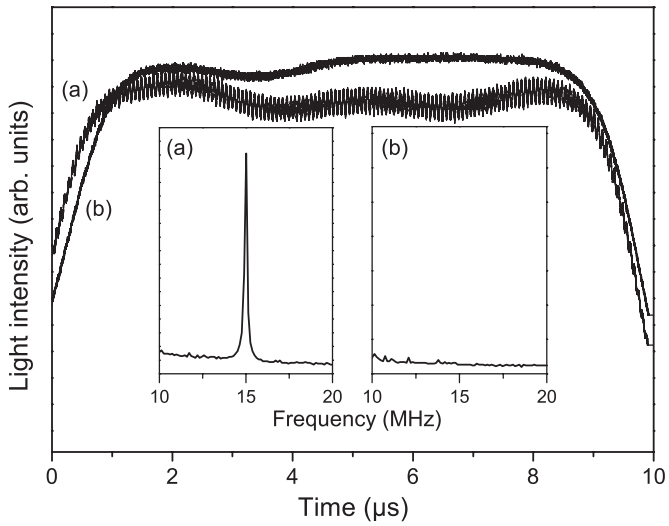

Figure 9. Raman echo heterodyne detection pulse in 0.2% Pr^{3+}:$La_2(WO_4)_3$. (a) Two-photon resonance. (b) 1 MHz detuning from two-photon resonance. Insets: Fourier transform of the signals. Raman pulse separation: 100 μs, T = 3.5 K.

(figure 6). The induced optical coherence was not absorbed since its frequency lies in the previously burned spectral hole (figure 8). When the spin coherence rephased, a beating at the hyperfine frequency was detected on the optical probe pulse, as shown in figure 9. The modulation amplitude was rather large, about 6% of the mean pulse amplitude for a 100 μs delay in the 0.2 at.%-doped sample. To confirm the nature of the observed beating, ω_1 frequency was shifted by 1 MHz resulting in the disappearance of the beating as can be seen on the Fourier transform of the pulse amplitudes (figure 9). This is due to the small inhomogeneous linewidth of the hyperfine transition, well below 1 MHz (see below). At short times, optical echoes created by each frequency in the two-colour pulses could have also produced beatings. However, since ω_2 frequency was very weakly absorbed and the two-colour pulses were long (3 μs) compared to the optimal optical echo ones (1 μs), such echo interferences were not

Table 1. Optical and hyperfine parameters for several Pr^{3+}-doped crystals.

Crystal	Y_2SiO_5(site 1) [25, 33, 34]	$YAlO_3$ [35–37]	$KY(WO_4)_2$ [38]	$La_2(WO_4)_3$	
Pr^{3+} conc. (at.%)	0.02	0.1	0.29	0.02	3
Pr^{3+} conc. (10^{19} ions cm^{-3})	0.38	2	1.8	0.16	23.4
Optical					
α (cm^{-1})	10		3.2	1.2	28
Γ_{inh} (GHz)	4.4	5	> 25	9	42
T_1 (μs)	164	160	43	64	3.5
Γ_h (kHz)	2.4	9.1	23.4	16	70
$T_2 = 1/(\pi\Gamma_h)$ (μs)	132.6	35	13.6	19.9	4.6
Hyperfine					
T_1 (s)	120	0.156	0.07	16	2
T_2 (μs)	550	366		250	250

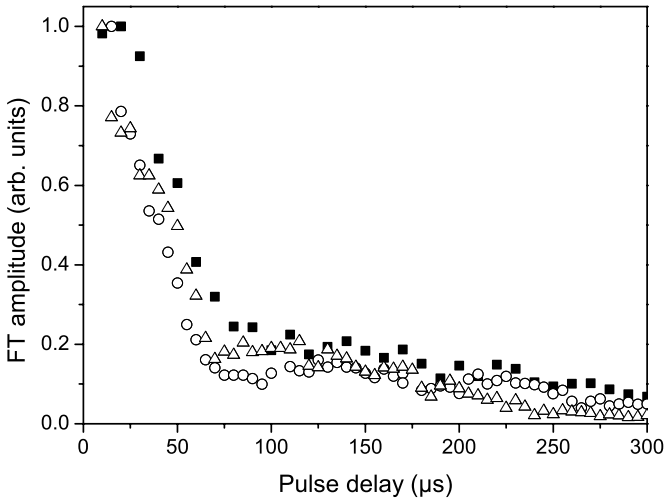

Figure 10. Raman echo decays as a function of Pr^{3+} concentration. Black squares: 0.02 at.%, open circles: 1.4 at.% and open triangles: 3 at.%.

observed. We could also observe Raman echoes without any hole burning, although at much lower amplitude, probably because the excitation pulse itself modifies hyperfine level populations.

Decays of the Fourier transforms of the probe pulse are presented in figure 10 as a function of the two-colour pulse delay and Pr^{3+} concentration. Two regimes can be observed as a function of time: a fast decay until 75 μs, attributed to the Raman free induction decay of the second two-colour pulse [21], and a longer one, corresponding to the Raman echo decay. Pr^{3+} concentration has little influence on these two parts. Exponential fits to each of them give hyperfine inhomogeneous and homogeneous linewidths of, respectively, 50 ± 2 and 1.27 ± 0.13 kHz. The latter corresponds to a coherence lifetime of 250 ± 30 μs. Some amplitude modulations can be observed on the Raman echo decay and could be due to superhyperfine interactions with La^{3+} nuclear spins.

In the case of the hyperfine transition, the population lifetime is very long even at high Pr^{3+} concentration (see above) and does not contribute to the homogeneous linewidth. The latter is then only due to spin–host interactions. As in the case of the optical coherence, figure 10 shows that the contribution of Pr^{3+}–Pr^{3+} interactions is low.

Table 1 summarizes optical and hyperfine parameters for several Pr^{3+}-doped oxide crystals. Taking into account that a typical π pulse lasts for about 1 μs with available laser intensities and the optical coherence is only used for transfer to the hyperfine one, it can be seen that all crystals have suitable optical parameters. Pr^{3+}:Y_2SiO_5 has however the advantage of a large oscillator strength. The hyperfine coherence lifetimes are also comparable but large differences appear for the hyperfine population lifetimes. Pr^{3+}:$YAlO_3$ and Pr^{3+}:$KY(WO_4)_2$ have hyperfine T_1^{hyp} in the 100 ms range, which make spectral tailoring difficult in these crystals. This is much easier in Pr^{3+}:$La_2(WO_4)_3$ even at high doping concentrations.

5. Conclusion

We have studied optical and hyperfine parameters relevant for quantum memories as a function of Pr^{3+} concentration in $La_2(WO_4)_3$ for the $^3H_4$–$^1D_2$ transition. The inhomogeneous linewidth Γ_{inh} was found to increase slowly with Pr^{3+} concentration due to the close ionic radii of Pr^{3+} and La^{3+}. This contributed to an increase of the peak absorption coefficient with increasing Pr^{3+} concentration, reaching 28 cm^{-1}at 3% doping level. Optical homogeneous linewidth decreased with Pr^{3+} concentration mainly because of the decrease in excited-state population lifetimes due to Pr^{3+}–Pr^{3+} energy transfers. At the highest Pr^{3+} concentration, the optical T_2 is 4.6 μs, still longer than a typical π pulse (1 μs). Hole lifetimes were also determined and gave average ground-state hyperfine level relaxation times in a 2–19 s range, allowing one to efficiently tailor the optical inhomogeneous linewidth by optical pumping. This important step is required by all quantum memory protocols. Finally, the ground-state $\pm 1/2$–$\pm 3/2$ hyperfine transition homogeneous and inhomogeneous linewidths were found to be essentially independent of Pr^{3+} concentration up to 3 at.%. This suggests that highly doped samples may be useful for high-efficiency quantum memories which require at the same time high optical densities and long storage times, i.e. long hyperfine coherence lifetimes.

Acknowledgments

This work is supported by the European Commission through the FP7 QuRep project and by the national grant ANR-07-BLAN-0273 Alacoqs.

References

[1] Macfarlane R M 2002 *J. Lumin.* **100** 1–20
[2] Böttger T, Thiel C W, Cone R L and Sun Y 2009 *Phys. Rev.* B **79** 115104
[3] Fraval E, Sellars M J and Longdell J J 2004 *Phys. Rev. Lett.* **92** 077601
[4] Lovric M, Glasenapp P, Suter D, Tumino B, Ferrier A, Goldner P, Sabooni M, Rippe L and Kröll S 2011 *Phys. Rev.* B **84** 104417
[5] Fraval E, Sellars M J and Longdell J J 2005 *Phys. Rev. Lett.* **95** 030506
[6] Nilsson M and Kroll S 2005 *Opt. Commun.* **247** 393–403
[7] Alexander A L, Longdell J J, Sellars M J and Manson N B 2006 *Phys. Rev. Lett.* **96** 043602
[8] de Riedmatten H, Afzelius M, Staudt M U, Simon C and Gisin N 2008 *Nature* **456** 773–7
[9] Damon V, Bonarota M, Louchet-Chauvet A, Chanelière T and Le Gouët J L 2011 *New J. Phys.* **13** 093031
[10] Hedges M P, Longdell J J, Li Y and Sellars M J 2010 *Nature* **465** 1052–6
[11] Afzelius M *et al* 2010 *Phys. Rev. Lett.* **104** 040503
[12] Chanelière T, Ruggiero J, Bonarota M, Afzelius M and Le Gouët J L 2010 *New J. Phys.* **12** 023025
[13] Saglamyurek E, Sinclair N, Jin J, Slater J A, Oblak D, Bussières F, George M, Ricken R, Sohler W and Tittel W 2011 *Nature* **469** 512–5
[14] Lauritzen B, Minář J, de Riedmatten H, Afzelius M, Sangouard N, Simon C and Gisin N 2010 *Phys. Rev. Lett.* **104** 080502
[15] Usmani I, Afzelius M, de Riedmatten H and Gisin N 2010 *Nature Commun.* **1** 1–7
[16] Clausen C, Usmani I, Bussières F, Sangouard N, Afzelius M, de Riedmatten H and Gisin N 2011 *Nature* **469** 508–11
[17] Afzelius M and Simon C 2010 *Phys. Rev.* A **82** 022310
[18] Könz F, Sun Y, Thiel C W, Cone R L, Equall R W, Hutcheson R L and Macfarlane R M 2003 *Phys. Rev.* B **68** 085109
[19] Shannon R D and Prewitt G T 1969 *Acta Crystallogr.* B **25** 925
[20] Guillot-Noël O, P Goldner, Le Du Y, Loiseau P, Julsgaard B, Rippe L and Kröll S 2007 *Phys. Rev.* B **75** 205110
[21] Guillot-Noël O, Goldner P, Beaudoux F, Le Du Y, Lejay J, Amari A, Walther A, Rippe L and Kröll S 2009 *Phys. Rev.* B **79** 155119
[22] Goldner P *et al* 2009 *Phys. Rev.* A **79** 033809
[23] Guillot-Noël O, Le Du Y, Beaudoux F, Antic-Fidancev E, Reid M, Marino R, Lejay J, Ferrier A and Goldner P 2010 *J. Lumin.* **130** 1557–65
[24] Holliday K, Croci M, Vauthey E and Wild U P 1993 *Phys. Rev.* B **47** 14741–52
[25] Equall R W, Cone R L and Macfarlane R M 1995 *Phys. Rev.* B **52** 3963–9
[26] Lauritzen B, Hastings-Simon S R, de Riedmatten H, Afzelius M and Gisin N 2008 *Phys. Rev.* A **78** 043402
[27] Afzelius M, Staudt M U, de Riedmatten H, Gisin N, Guillot-Noël O, Goldner P, Marino R, Porcher P, Cavalli E and Bettinelli M 2010 *J. Lumin.* **130** 1566–71
[28] Macfarlane R M and Shelby R M 1987 *Spectroscopy of Solids Containing Rare Earth Ions* ed A A Kaplyanskii and R M Macfarlane (Amsterdam: North-Holland) p 51
[29] Inokuti M and Hirayama F 1965 *J. Chem. Phys.* **43** 1978
[30] Hartmann S 1968 *IEEE J. Quantum Electron.* **4** 802–7
[31] Louchet A, Du Y L, Bretenaker F, Chanelière T, Goldfarb F, Lorgeré I, Le Gouët J L, Guillot-Noël O and Goldner P 2008 *Phys. Rev.* B **77** 195110
[32] Alexander A L, Longdell J J and Sellars M J 2007 *J. Opt. Soc. Am.* B **24** 2479–82
[33] Ham B S, Shahriar M S, Kim M K and Hemmer P R 1998 *Phys. Rev.* B **58** R11825–8
[34] Nilsson M, Rippe L, Kröll S, Klieber R and Suter D 2004 *Phys. Rev.* B **70** 214116
[35] Macfarlane R M, Shelby R M and Shoemaker R L 1979 *Phys. Rev. Lett.* **43** 1726–30
[36] Erickson L E 1991 *Phys. Rev.* B **43** 12723–8
[37] Klieber R, Michalowski A, Neuhaus R and Suter D 2003 *Phys. Rev.* B **68** 054426
[38] Xu H L, Nilsson M, Ohser S, Rauhut N, Kröll S, Aguiló M and Díaz F 2004 *Phys. Rev.* B **70** 214115